Article

Study on Creep Characteristics of Water Saturated Phyllite

Yabin Wu [1,2], Jianhua Hu [3,](ID) and Guanping Wen [4,]

1   Changsha Institute of Mining Research Co., Ltd., Changsha 410012, China
2   State Key Laboratory of Safety Technology of Metal Mine, Changsha 410012, China
3   Zijin School of Geology and Mining, Fuzhou University, Fuzhou 350108, China
4   School of Resources and Safety Engineering, Central South University, Changsha 410083, China
*   Correspondence: hujh21@csu.edu.cn (J.H.); guanping-wen@csu.edu.com (G.W.)

Abstract: Phyllite is affected by its own bedding, stress environment and water-saturated conditions. There are great differences in its deformation and failure in engineering, and its creep characteristics are an important basis for evaluating the long-term stability of phyllite engineering. Therefore, this study carried out creep tests of water-saturated phyllite under different bedding angles and confining pressures, studied the coupling effect of factors that affect the creep characteristics of phyllite, and investigated and analyzed the deformation characteristics of a phyllite roadway support on site to provide basic support for phyllite roadway mine disaster control and collaborative mining research. The results showed the following: (1) When the bedding dip angle was 30~60°, under the control of the bedding, the sliding deformation along the bedding suddenly increased under the low-stress condition and the specimen did not undergo structural damage. It could continuously bear multi-level stress and generated creep deformation. In this case, a phyllite roadway should adopt the support method of combining flexibility and rigidity. (2) In the process of multi-stage stress loading, the creep instantaneous stress was directly proportional to the initial stress. When the stress was loaded to 50% of the failure strength, the instantaneous stress tended to be stable and maintained a linear, slightly increasing relationship with the stress. When the bedding angle was 30~60°, the creep deformation accounted for more than 50% of the total deformation. The bedding angles of 0° and 90° were dominated by the instantaneous strain during the stress loading process. For the flexible support of the roadway, the deformation caused by disturbance stress should be fully considered. (3) The uniaxial creep specimen mainly displayed compression shear tensile failure, with a small number of parallel cracks along the main fracture surface. The triaxial creep fracture mode changed to single shear failure. The confining pressure showed greater inhibition of the creep of the specimen with a bedding inclination of 0° and 90°. The strength design of the rigid support should refer to the original rock stress value of the roadway. The creep deformation and failure of the specimen with a bedding inclination of 30~60° were mainly controlled by the bedding. The included angle between the bedding dip angle and the maximum principal stress should be kept within 30~60° as far as possible in the roadway layout.

Keywords: phyllite; rock mechanics; roadway support; stress environment; creep characteristics

1. Introduction

Phyllite is a common rock type in engineering, and its large deformation characteristics make it the main factor that affects the safety and stability of tunnels, shafts and side slopes containing phyllite [1]. Because phyllite generally contains clay minerals with strong water absorption, it is easy to reach the water-saturated state in a water-containing environment [2]. At this time, the mechanical properties are greatly reduced. At the same time, the layered structure makes the anisotropy of phyllite prominent [3], and different stress sizes and directions have a serious impact on the mechanical behavior of phyllite. Therefore, it is important to study the coupling creep characteristics of water-saturated

phyllite bedding and the associated stress conditions to guide the stability analysis of phyllite engineering design and construction safety [4].

In view of the above problems, scholars at home and abroad have carried out a lot of research. T. Ramamurthy [5] carried out compression tests on quartz phyllite, carbonaceous phyllite and mica phyllite; obtained the relationship between the strength and dip angle of different phyllites; and quantitatively analyzed the anisotropy according to the measurement parameters. The results showed that the anisotropy curves of the three phyllites were U-shaped. Ziquan Chen et al. [6] carried out uniaxial and triaxial compression tests on sericite phyllite and found that under uniaxial compression, the peak strength, elastic modulus and bedding dip angle showed a U-shaped relationship, and each parameter showed a linear increasing trend under triaxial compression. Through a uniaxial compression acoustic emission test of phyllite, Xuefeng Si et al. [7] found that peak stress, peak strain, cumulative acoustic emission count and elastic strain potential energy all showed a U-shaped change trend with the bedding dip angle. Jianjun Zhao et al. [8] studied the conventional triaxial compression test of phyllite with different water saturation times and found that the relationship between mechanical parameters and water saturation time of phyllite decreased nearly linearly within 60 days of water saturation. After 60 days, the parameter value did not change, the deformation was transformed from elasticity to plasticity, and the aging property of parameter degradation first increased and then decreased. X Chang [9] undertook triaxial compression tests of phyllite under different confining pressures. The results showed that under the condition of low confining pressure, phyllite mainly demonstrated tensile shear failure, while high confining pressure changed this into shear failure. The relationship between maximum principal stress and confining pressure was established, and the general angle of a phyllite shear failure surface was proposed. In terms of research on the creep characteristics of phyllite, Guowen Xu [10] carried out uniaxial compression creep tests of carbonaceous phyllite at different bedding angles in a water-containing state, analyzed the influence of bedding inclination on its creep characteristics and established a layered rock mass creep model; however, the model could not reflect the changes of mechanical parameters of phyllite under different stress conditions. Cheng Lyu [11] studied the creep parameters of phyllite under triaxial variable confining pressure step loading with different bedding dip angles, described the test results with Burger's creep model, and established the function of phyllite bedding dip angle, confining pressure and creep parameters, but did not consider the influence of water saturation on phyllite. Discenza, Marco Emanuele [12] studied the graded loading creep characteristics of carbon phyllite under different confining pressure conditions, established the creep constitutive model of carbon phyllite through the improved Masao Nishihara model and applied the model to the development of new support structures for controlling the stability of anti-coupled rheological surrounding rocks, mainly considering the creep characteristics of phyllite under the influence of different stress environments. Linjian Ma [13] studied the creep characteristics of Sericite phyllite under different confining pressures under graded loading, found that the lateral rheological deformation and rate were greater than for the axial axis, and expounded the rheological dilatancy mechanism. Through a phyllite rheological test, Guowen Xu [14] found that a failure mode dominated by shear under long-term action can creep under the condition of small stress; a phyllite creep model was developed based on Burger's model without considering the influence of the water state on the mechanical properties of the phyllite.

The above research results were mainly from the experimental study of instantaneous and creep mechanical properties. Among them, the influence of instantaneous mechanical properties on the mechanical properties of phyllite under bedding, water content conditions and a stress environment is clear. However, the study of long-term mechanical behavior characteristics under bedding, water saturation and stress conditions using phyllite creep tests is insufficient, and the coupling of influencing factors should be comprehensively considered to study the creep properties of phyllite. Therefore, in view of the long-term creep characteristics of water-saturated phyllite, it is necessary to study the creep characteristics

of the bedding, confining pressure and water-saturated conditions to provide theoretical support for the long-term stability of a phyllite roadway support.

2. Materials and Methods

2.1. Sample Preparation

Phyllite samples were taken from large phyllite regions with clear and uniform bedding in the engineering rock mass, and the rock samples were processed into Φ 50 mm $\times$ 100 mm cylinders; the error of the two end faces was controlled to within ±0.05 mm and the perpendicularity of the two end faces was controlled to within $\pm0.25°$. At the same time, the phyllite block was processed into test rock samples with different bedding dip angles, where the bedding dip angle β is the angle between the horizontal plane and the bedding plane. In order to make the study representative and typical, the bedding dip angle β was set to five angles: 0°, 30°, 45°, 60° and 90°. Samples are shown in Figure 1.
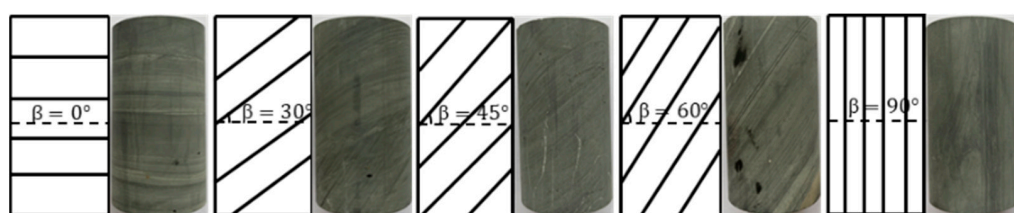

Figure 1. Different bedding dip angles of phyllite rock samples.

2.2. Testing System

An MTS815 rock mechanics test system was used to carry out uniaxial and triaxial creep tests of the saturated phyllite. The MTS815 loading test and recording system are shown in Figure 2. The axial stress mode of step loading was adopted, and the axial stress was loaded step by step according to the set stress series until the specimen was destroyed. The range of axial stress grading was 35–85% of the uniaxial compressive strength [15]. Through the uniaxial compression test, it was found that the compressive strengths of samples with different bedding angles were quite different. The compressive strengths of rock samples with bedding angles of 0° and 90° were close, and those of 30°, 45° and 60° were close. In order to compare the creep characteristics of rock samples with different bedding angles under the same stress condition, the classification of axial loading stress should be as unified as possible. Therefore, the experiment was divided into two different stress loading levels [16]. See Table 1 for the test plan. The loading rate was 0.04 kN/S, and the creep time of each level of the load was 7200 s. The automatic loading of the program was set. When the loading time of each level reached this time, the next level of loading was used. The protection of the test system was set such that the loading could be automatically stopped after the sample was destroyed.
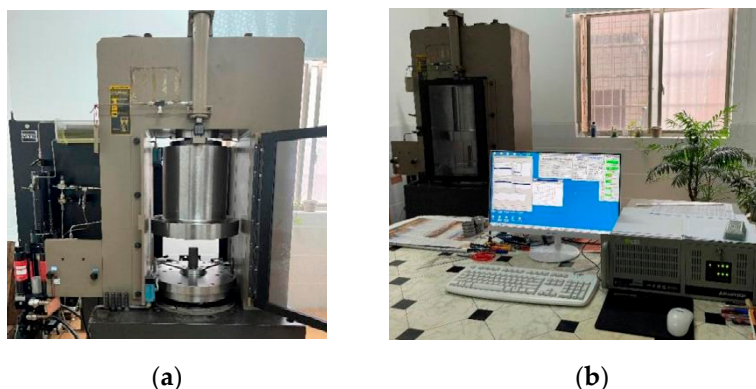

(**a**)   (**b**)

Figure 2. MTS-815 loading test and recording system: (**a**) test system and (**b**) recording system.

Table 1. Test plan.

Group	Confining Pressure (MPa)	β (°)	Loading Stress Level σ1 (MPa)	Duration of Each Level of Load (s)
1	0	0, 90	28, 36, 44, 52, 60, 68, 76, 84	7200
		30, 45, 60	6, 9, 12, 15, 18, 21, 24, 27	
2	15	0, 90	65, 80, 95, 110, 125, 140, 155	7200
		30, 45, 60	20, 28, 36, 44, 52, 60, 68, 76	

3. Results and Discussion

3.1. Creep Time–Axial Strain Curve

The above creep test was completed and the creep time–axial strain curve of each sample was obtained, as shown in Figure 3.

(1) In the process of multi-level stress loading, during the first level loading, due to the pores in the rock and the expansion of kaolinite after being saturated with water, the internal space of the sample was compacted under the load and the instantaneous stress of the sample was significantly greater than that of the later loading process. The maximum axial stress of the compaction process was displayed by the 0° bedding sample, and the minimum was for the 90° bedding sample. When the initial load was completed and the axial stress was loaded in the later stages, the creep deformation increased rapidly at first. After the loading was completed, the creep rate decreased rapidly, and the displacement remained unchanged. The creep rate was close to zero and entered the constant speed creep stage. Under the application of the last level of stress, there were three obvious stages of slow creep, constant speed creep and accelerated creep, where the 0° and 30° bedding specimens were more prominently affected, and the accelerated creep stage of the 90° bedding specimen was not obvious, which reflected its brittleness.

(2) Compared with the failure strength of all the creep samples, the water-saturated phyllite samples with bedding angles of 0°, 30°, 45°, 60° and 90° were subjected to uniaxial creep tests at the stress levels of 52 MPa, 12 MPa, 27 MPa, 21 MPa and 87 MPa (when the 84 MPa grade was completed and ready to be loaded into the next grade), along with the triaxial creep tests at the stress levels of 128 MPa, 45 MPa, 44 MPa, 52 MPa and 142 MPa. Under the same bedding angle, the triaxial creep failure strength was obviously greater than the uniaxial creep failure strength. Under the confining pressure, the triaxial creep strength increased by a larger factor than the uniaxial creep strength for the 30° bedding specimen.
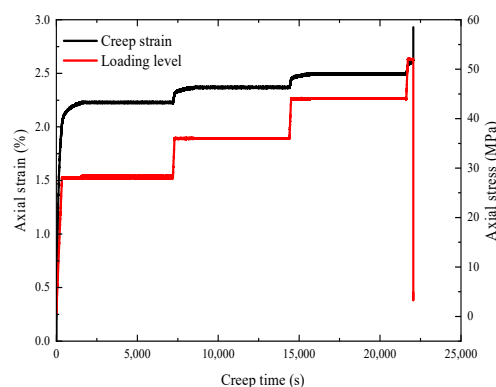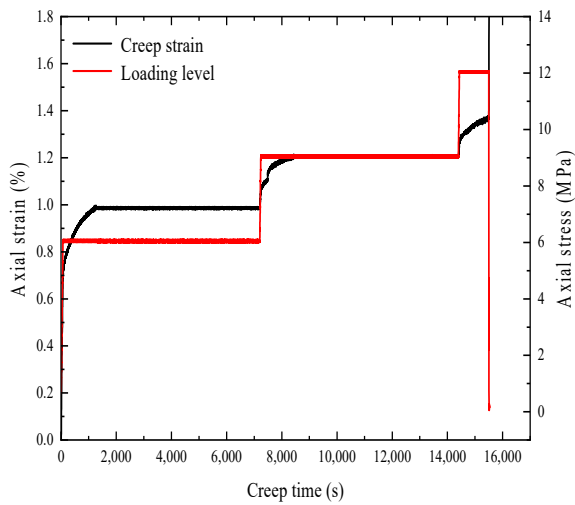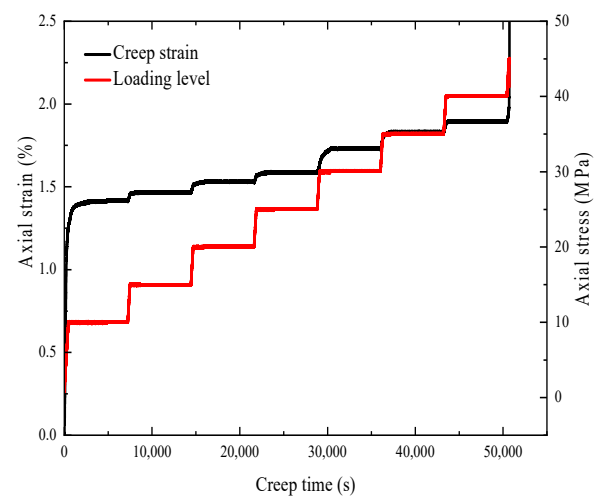
(**a**) 0 MPa confining pressure.
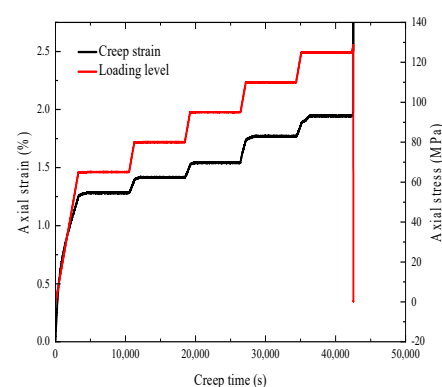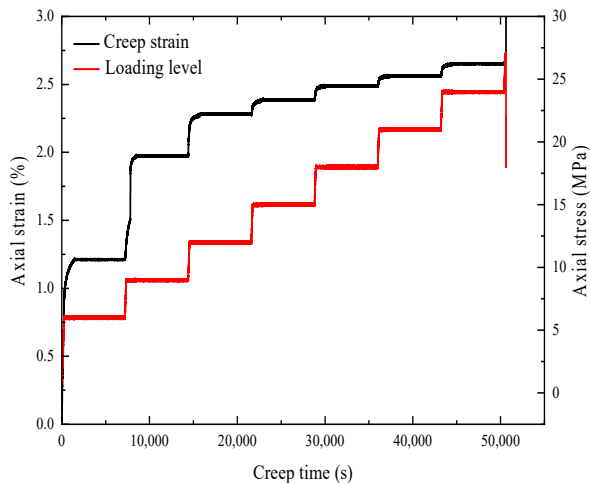
(**b**) 15 MPa confining pressure.

(**1**) β = 0°.

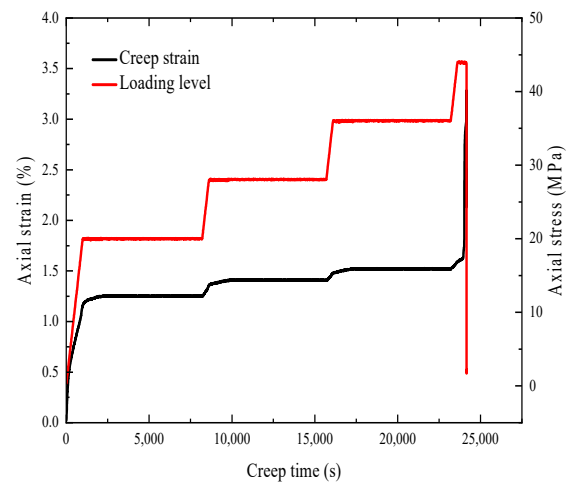**Figure 3.** *Cont.*

(**a**) 0 MPa confining pressure.

(**b**) 15 MPa confining pressure.
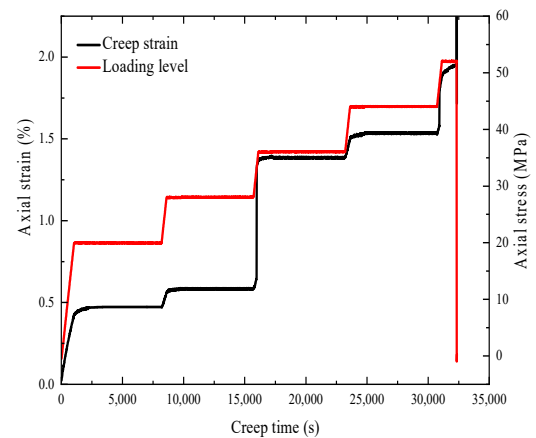
(**2**) β = 30°.

(**a**) 0 MPa confining pressure.

(**b**) 15 MPa confining pressure.

(**3**) β = 45°.
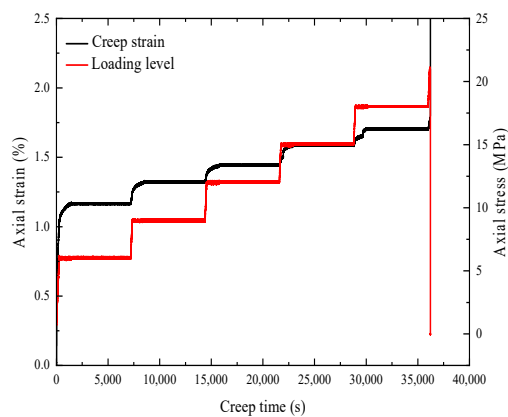
(**a**) 0 MPa confining pressure.

(**b**) 15 MPa confining pressure.

(**4**) β = 60°.

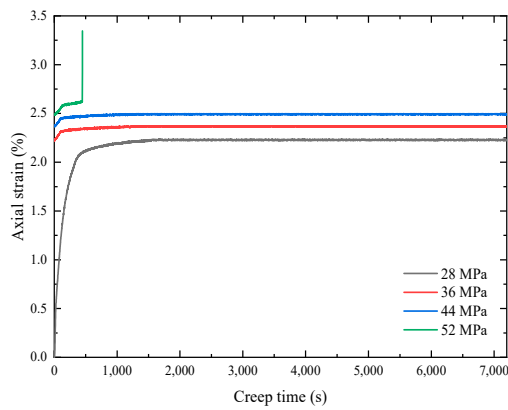**Figure 3.** *Cont.*
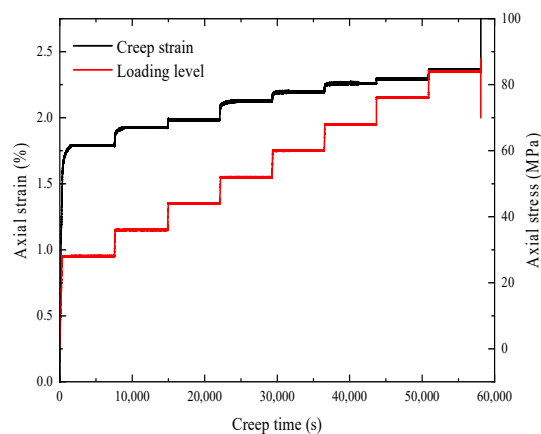
(**a**) 0 MPa confining pressure.
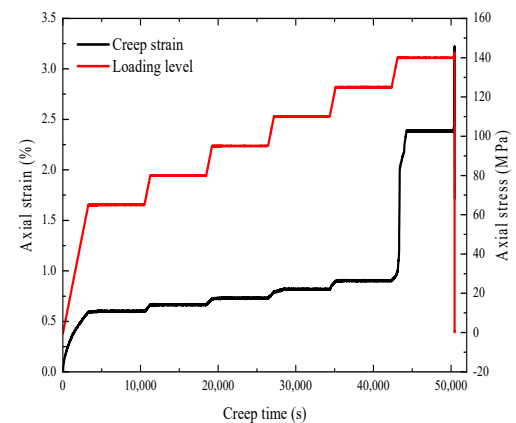
(**b**) 15 MPa confining pressure.

(**5**) β = 90°.

Figure 3. Time–strain curve of the creep test under different bedding inclinations and confining pressures.

3.2. Relationship between Strain and Time

The Boltzmann superposition principle was used to process the test data, and the creep strain versus time curves of different beddings were obtained [17–19], as shown in Figure 4.

(1) The sum of the first three grades of creep stress under stress loading was the largest, and the creep phenomenon was obvious. The uniaxial compression creep stress of the 45° bedding specimen was the largest, and its creep deformation mainly occurred at the first two stress levels. The next creep strain was the 30° bedding specimen, which also had a large creep deformation at 9 MPa. The maximum stress of the 90° bedding specimen occurred near the last loading stress level. The main reason for this was that the 90° bedding specimen had the smallest compressible space, and its stress variable was the crack before the failure.

(2) Under the low-stress condition, the creep process occurred along the bedding. In the creep curves of the specimens with 30°, 45° and 60° bedding angles, it can be seen that the deformation suddenly increased when the stress load was constant, especially for the specimen with 45° bedding. When the axial stress was a 9 MPa dead load, the axial deformation suddenly increased in the creep attenuation stage, and the strain increased by about 0.4%. The specimen with a 30° bedding angle had the same situation at 9 MPa. Similar situations occurred at 15 MPa and 18 MPa for the specimen with a bedding inclination of 60°, but the specimen did not undergo structural damage or the subsequent sustainable bearing capacity creep. The main reason for this phenomenon was the appearance of bedding control.
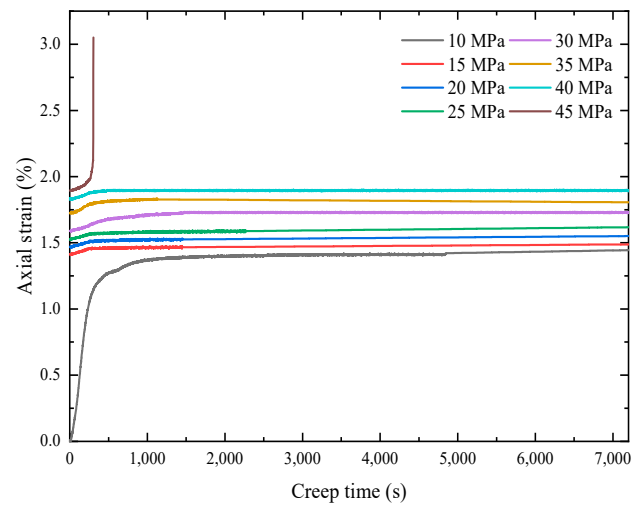
(**a**) 0 MPa confining pressure.
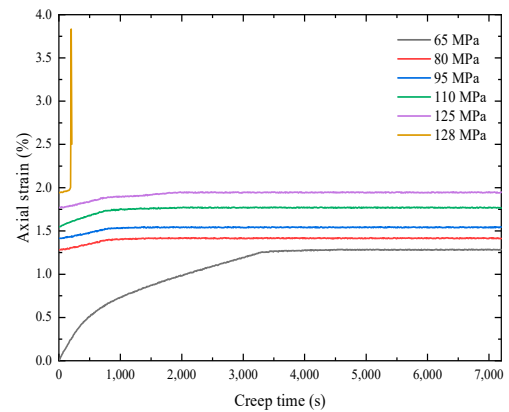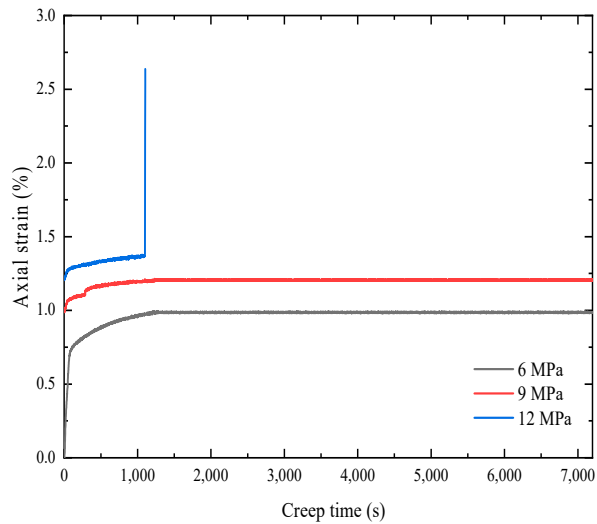
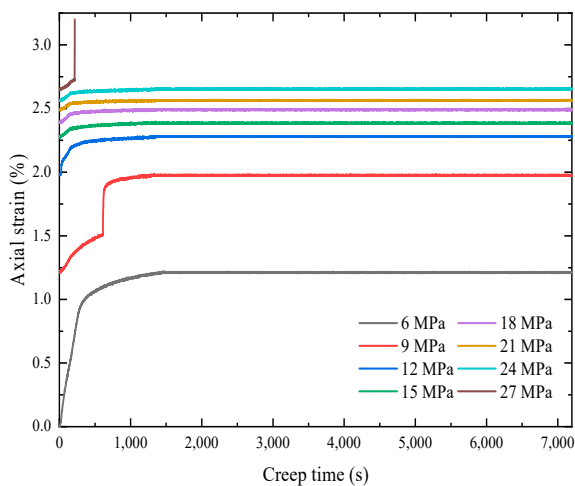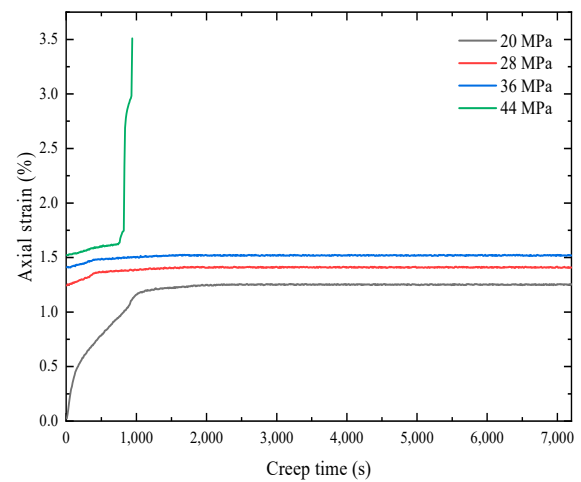(**b**) 15 MPa confining pressure.

(**1**) β = 0°.

(**a**) 0 MPa confining pressure.

(**b**) 15 MPa confining pressure.

(**2**) β = 30°.

(**a**) 0 MPa confining pressure.

(**b**) 15 MPa confining pressure.

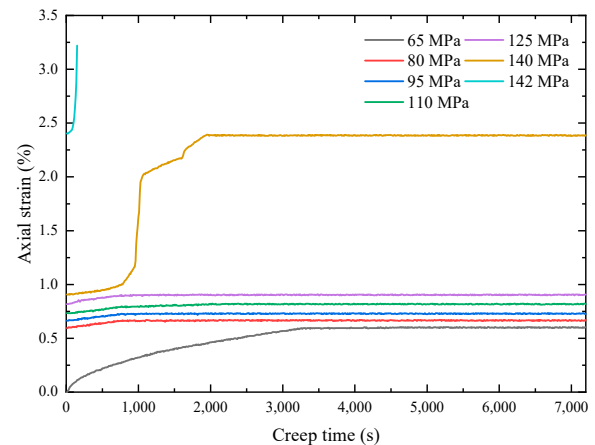(**3**) β = 45°.

Figure 4. *Cont.*
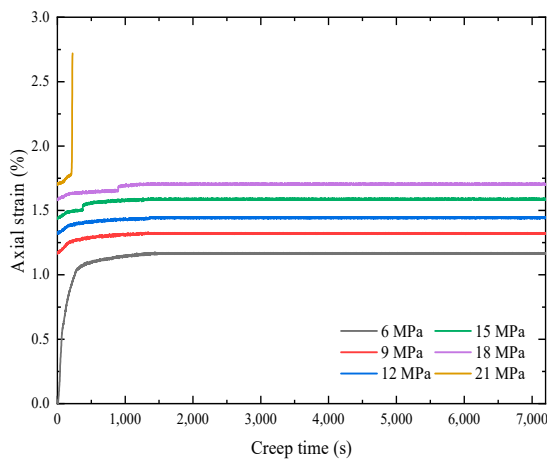
(**a**) 0 MPa confining pressure.
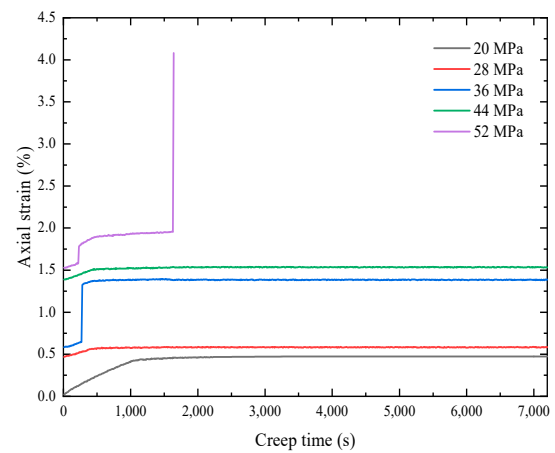
(**b**) 15 MPa confining pressure.

(**4**) β = 60°.
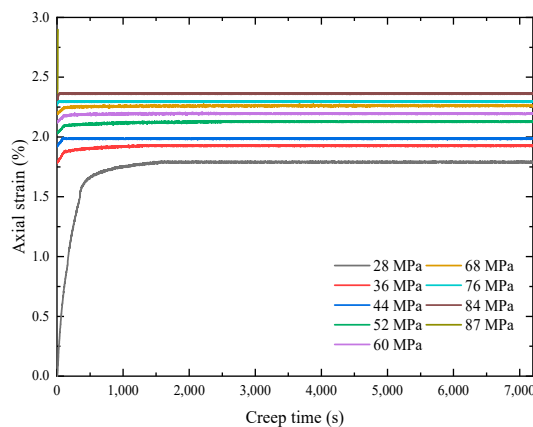
(**a**) 0 MPa confining pressure.

(**b**) 15 MPa confining pressure.

(**5**) β = 90°.

Figure 4. Axial creep strain versus time at each loading level.

3.3. Instantaneous Strain and Creep Strain

The instantaneous stress variable is the stress variable produced in the process of loading stress, which is closely related to the stress environment. The creep stress variable is the stress variable that changes with the loading time when the stress is constant, which can reflect the mechanical behavior of different stress loading times. As for the proportion of the instantaneous stress variable and creep stress variable in the total strain, it directly affects the engineering deformation and support design of phyllite. As shown in Figure 5, the deformation magnitude of the instantaneous strain and creep strain could be separated from the identification diagram.

According to Figure 5, the strain and bedding dip angle were separated and the relationship curve was drawn, as shown in Figures 6–8. From the comparison of instantaneous stress variables and creep stress variables of different bedding dip angles in Figures 6 and 7, it can be seen that the instantaneous strain was the largest when loading the first three stress levels, of which the maximum stress variable was found for the 0° bedding sample, followed by the 90° sample, which was caused by the large instantaneous loading stress value of the first level. Under the loading stress of the same level for 0° and 90°, the 0° bedding instantaneous strain was greater than that of the bedding angle of 90°. This shows that the deformation of the 0° laminated specimen was the largest in the compaction stage.

Similarly, when the 30°, 45° and 60° laminated samples were loaded with the first stress level, the instantaneous strain of the 60° laminated sample was the largest, but when the second level was loaded, the instantaneous deformation of 45° laminated sample increased rapidly, and the instantaneous strains of the 30° and 60° laminated samples were close. In general, the instantaneous strain after the three stress levels tended to be stable, maintaining a small, linearly increasing relationship with the stress level. In the creep process, the instantaneous stress was directly proportional to the magnitude of the loading stress. It can be seen from Figure 8 that under the same loading level, the instantaneous elastic modulus increased with the increase in loading stress. The elastic modulus was the largest during creep failure, and the instantaneous elastic modulus was linear with the magnitude of the loading stress. When the bedding inclination angle was the same, the larger the confining pressure was, the larger the instantaneous elastic modulus; the confining pressure had the most obvious effect on the bedding inclination angle of 90°, followed by the 0° bedding; and the confining pressure had little effect on the change of the instantaneous elastic modulus of 30°.
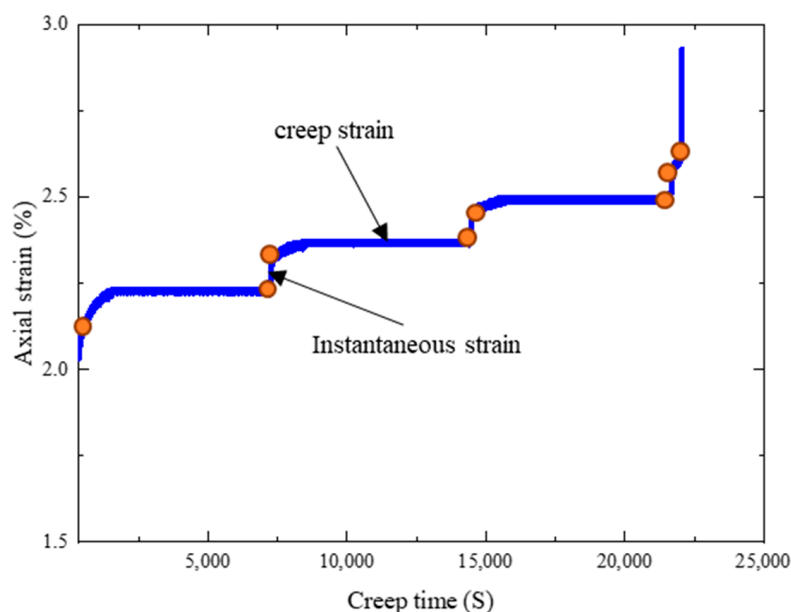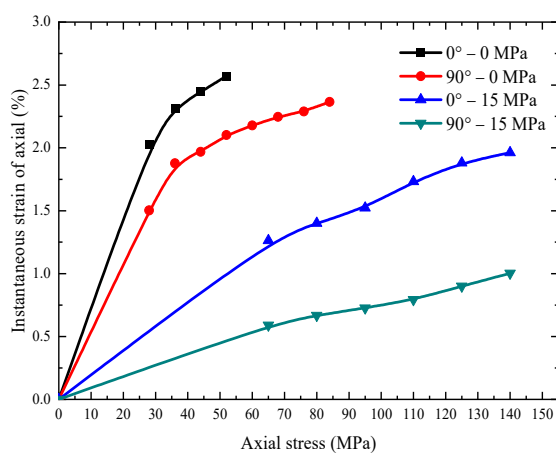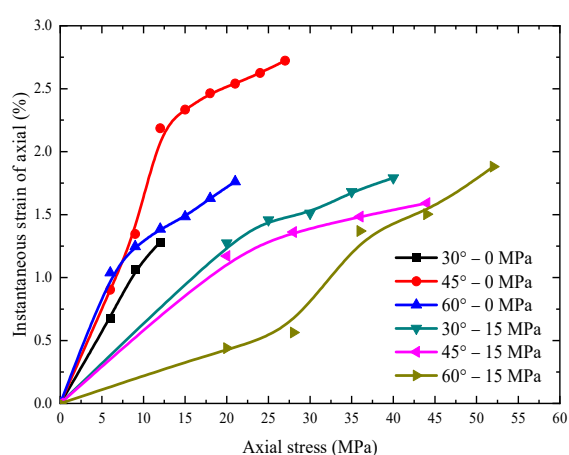

Figure 5. Identification diagram of the instantaneous strain and creep strain.

(**1**) β = (0°, 90°).

(**2**) β = (30°, 45°, 60°).

Figure 6. Comparison of the instantaneous strain.

(**1**) β = (0°, 90°).

(**2**) β = (30°, 45°, 60°).
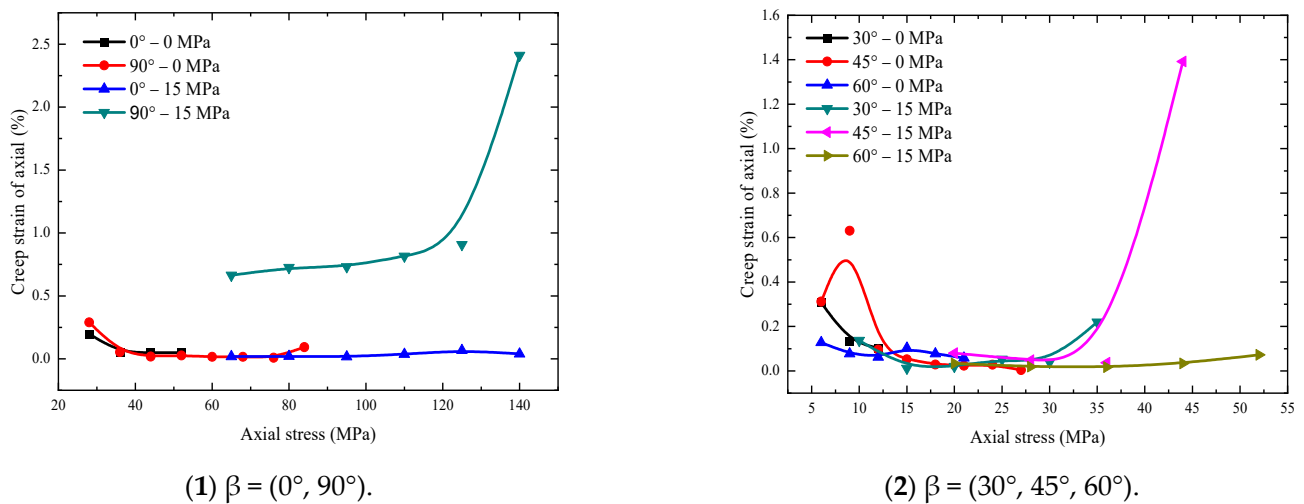
Figure 7. Comparison of the creep strain.

(**1**) β = (0°, 90°).

(**2**) β = (30°, 45°, 60°).
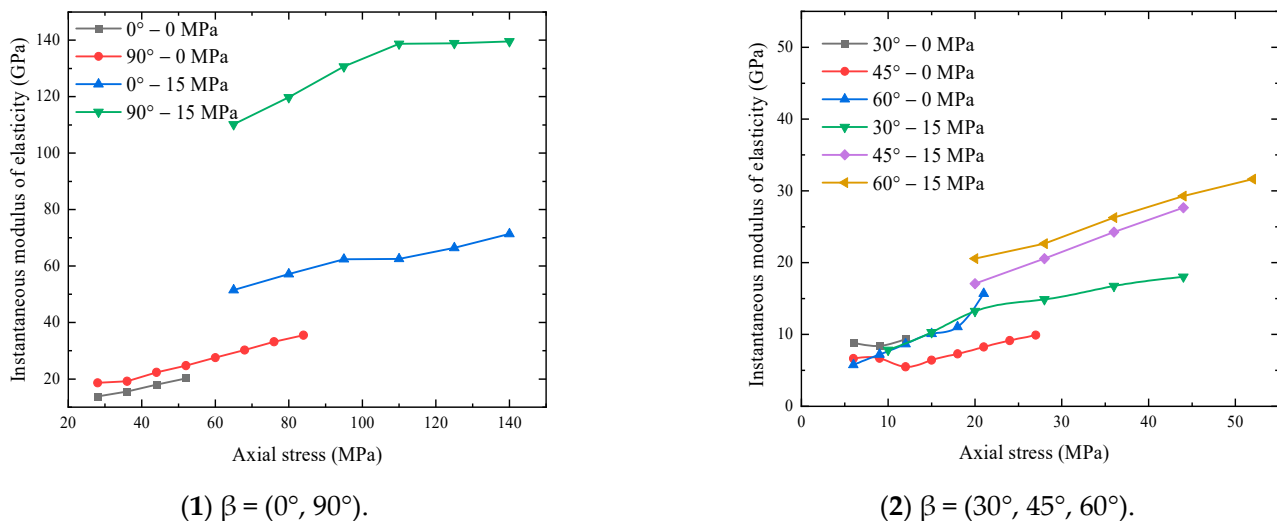
Figure 8. Comparison of the instantaneous elastic modulus.

3.4. Failure Strength

Figure 9 shows the uniaxial and triaxial creep stress–strain curves with different bedding dip angles, while Figure 10 gives a comparison of the curves of creep failure strength and instantaneous failure strength.

From the uniaxial creep results, it can be seen that the bedding dip angle of 0° was loaded with the same stress level as that of 90°. The bedding dip angle of 0° was destroyed at the fourth level, and the failure stress level was 52 MPa, which was 74.29% of the instantaneous strength (70 MPa), while the 90° bedding was destroyed at the ninth level after eight levels of loading, and the stress at the time of failure was 87 Mpa, which was 94.29% of the instantaneous strength (92 MPa). The same stress was applied to the bedding dip angles of 30°, 45° and 60°. The bedding dip angle of 30° showed third-grade failure, and the failure stress grade was 12 MPa, which was 75% of the instantaneous strength (16 MPa). The 45° bedding was destroyed during the loading of the eighth grade, and the failure stress grade was 27 MPa, which was 77% of the instantaneous strength (35 MPa). The 60° bedding was destroyed during the loading of the sixth grade, and the failure stress grade was 21 MPa, which was 84% of the instantaneous strength (25 MPa). Therefore, the statistical analysis of the ratio of creep failure strength to instantaneous strength showed that there were great differences in the influence of creep on the strength of phyllite with different bedding angles. The influence of creep on the failure strength of the samples with

different bedding angles was ordered according to 0° > 45° > 30° > 60° > 90°. From the perspective of the creep failure strength of the 90° bedding sample, the creep effect was small, and the creep deformations of the first two grades of creep failure were the smallest and close. Creep had the least effect on its mechanical properties, which further showed that bedding had greater control on the creep strength of phyllite.
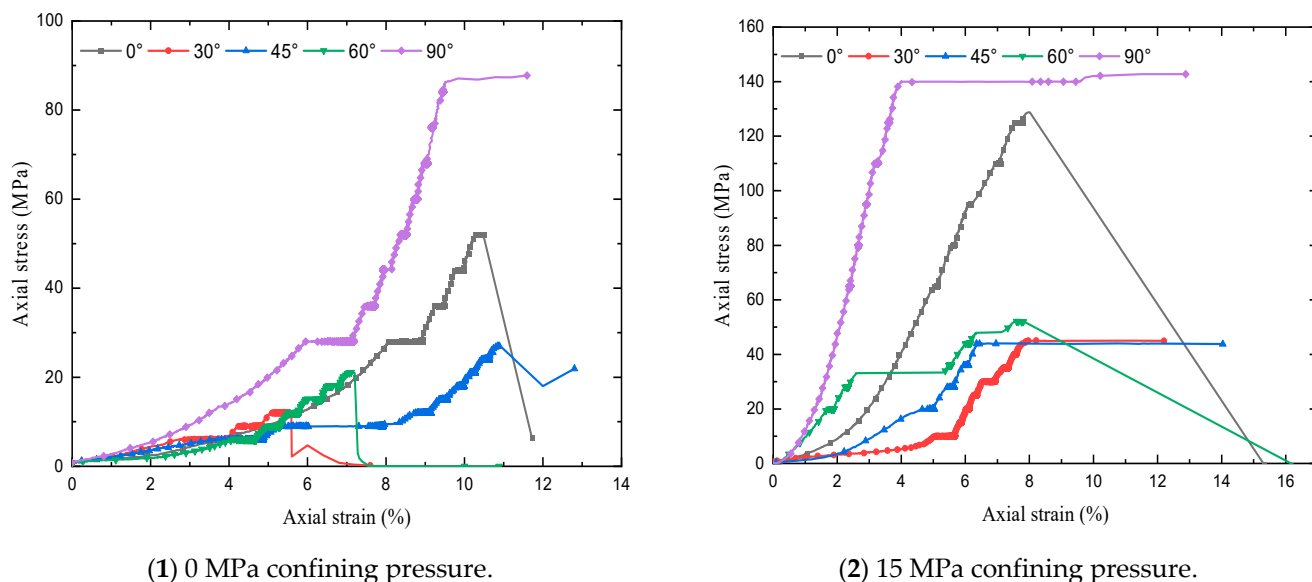

(**1**) 0 MPa confining pressure.　　　(**2**) 15 MPa confining pressure.

Figure 9. Stress–strain curve of the creep test under different bedding inclinations and confining pressures.
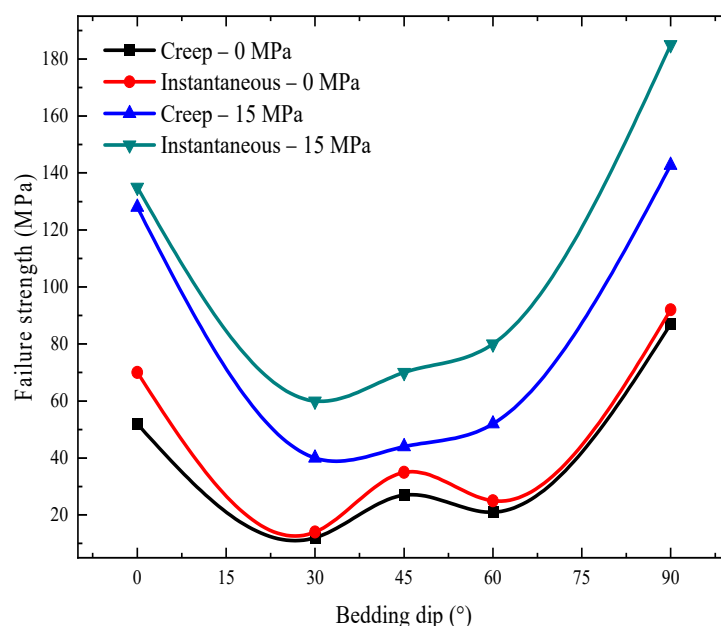
Figure 10. Comparison between the creep failure strength and instantaneous failure strength.

From the triaxial creep test results, it can be seen that the bedding dip angles of 0° and 90° were loaded with the same stress level. The 0° dip angle was destroyed at the sixth level, and the destruction stress level was 127.5 MPa, which was 96.24% of the instantaneous strength (133 MPa), while the 90° bedding was destroyed at the seventh level, and the stress at the time of destruction was 142.7 MPa, which was 68.6% of the instantaneous strength (208 MPa). The bedding dip angles of 30°, 45° and 60° were loaded with the same stress. The bedding dip angle of 30° showed eighth-grade failure, and the failure stress grade was 45 MPa, which was 84.9% of the instantaneous strength (53 MPa). The 45° bedding was

damaged during the loading of the fourth grade, and the failure stress grade was 44 MPa, which was 67.69% of the instantaneous strength (65 MPa). The 60° bedding was damaged during the loading of the fifth grade, and the failure stress grade was 52 MPa, which was 69.33% of the instantaneous strength (75 MPa). Therefore, the influence of creep on the failure strength of samples with different bedding dip angles was ordered according to 45° > 90° > 60° > 30° > 0°. Under triaxial creep, the bedding dip angles of 0° and 90° and uniaxial creep appeared in obvious contrast, and the ratio of the triaxial creep failure strength to its instantaneous strength decreased. The confining pressure had a greater inhibitory effect on the failure of samples with bedding dip angles of 0°~30°.

3.5. Creep Failure Mode

See Table 2 for the failure morphology of the creep test samples. It can be seen from the table that there were also obvious differences in the creep failure morphologies of the water-saturated phyllite under uniaxial and triaxial conditions. Under uniaxial compression, the failure mode of the specimen was compression shear tension failure, with a small number of parallel cracks along the main fracture surface. When the triaxial confining pressure was 15 MPa, the fracture form of the specimen changed to a single shear failure. Due to the creep action, the damage accumulation of the bedding plane produced a fracture surface, and the sliding along the fracture surface formed a shear surface, which led to the destruction of the specimen, and there were friction cracks on the shear surface [20–22].

Table 2. Creep failure mode.

Confining Pressure Level	Creep Test Failure Mode of Phyllite with Different Dip Angles				
	0°	30°	45°	60°	90°
0 MPa					
	Shear slip and tension	Shear slip and tension	Shear slip	Shear slip and tension	Mainly parallel cutting
15 MPa					
	Shear failure	Shear slip	Shear slip	Shear slip	Mainly parallel cutting

4. Engineering Examples

The main factors that affected the deformation and failure of phyllite were obtained through the early creep test of saturated phyllite. In order to compare the test results with the differences in engineering, the deformation process of a phyllite roadway support structure in a lead–zinc mining area was tracked, monitored and analyzed. The roadway support methods were a roof-leading small steel pipe + I-shaped steel, roof-leading small steel pipe + track steel frame, wood support + I-shaped steel, steel frame + concrete shotcrete layer, etc. During the above support, the excavated face was closed in time to prevent the surrounding rock from weathering. However, most of the support steel frames experienced large deformations. The deformation and failure modes included the sinking and bending of I-steel beams caused by top pressure, as well as the deformation of I-steel and the extrusion and bulging of the bottom corners caused by side pressure. The service life of most of the support areas with large deformation was about 1–6 months. The roadway had a short service life and a high repair rate. The specific deformation and failure characteristics of the roadway support structure were as follows [23–26].

(1)　The deformation speed of the deep roadway support steel frame was fast and the deformation was large.

With the increase in the mining depth of the roadway, the deformation amount and deformation speed of the surrounding rock of the roadway increased. After the rapid deformation of the surrounding rock of the free roadway face after the excavation, it gradually became stable. It was necessary to support and control the deformation of the surrounding rock as soon as possible, and the steel frame slowly deformed after the support based on the steel frame. As shown in Figure 11a,b, the roof sunk and the roof steel frame bent and deformed. When the roadway was mined to the middle section below 500 m, the stability of the free surface after the roadway excavation became poor and deformed rapidly. The deformation speed was significantly higher than that after the excavation of the upper middle section of the roadway. It was necessary to increase the advanced support bolts to ensure the safety of the blasting hole construction. The blast hole in the roadway excavation was seriously deformed, and the deformation occurred about two hours after the completion of blast hole construction. The blast hole became oblate, and the deformation speed was significantly higher than that of the shallow surrounding rock.

(2)　The creep characteristics of the surrounding rock were obvious, and the horizontal deformation of the roadway support steel frame was serious.

With the increase in mining depth, the continuous deformation of the roadway support structure was significant, that is, the rheological property of the surrounding rock was obvious. It can be seen that the creep characteristic of phyllite was the main reason for the deformation of the roadway support structure. In the middle section of 500 m, the roadway support adopted the same support structure and parameters as the upper-middle section, and the deformation of the roadway side slope was obvious, as shown in Figure 11c,d. The steel frame deformation occurred at the foot of the roadway support steel frame and the center of the side slope, and the deformation duration of its steel frame support body increased significantly, which was mainly reflected in the increase in repair times, and the steel frame deformation occurred every 6 months on average. Under the action of horizontal stress, the roadway bulged out from the two leg supports, and the track steel support was damaged, which occurred at the connection of the two steel frames.
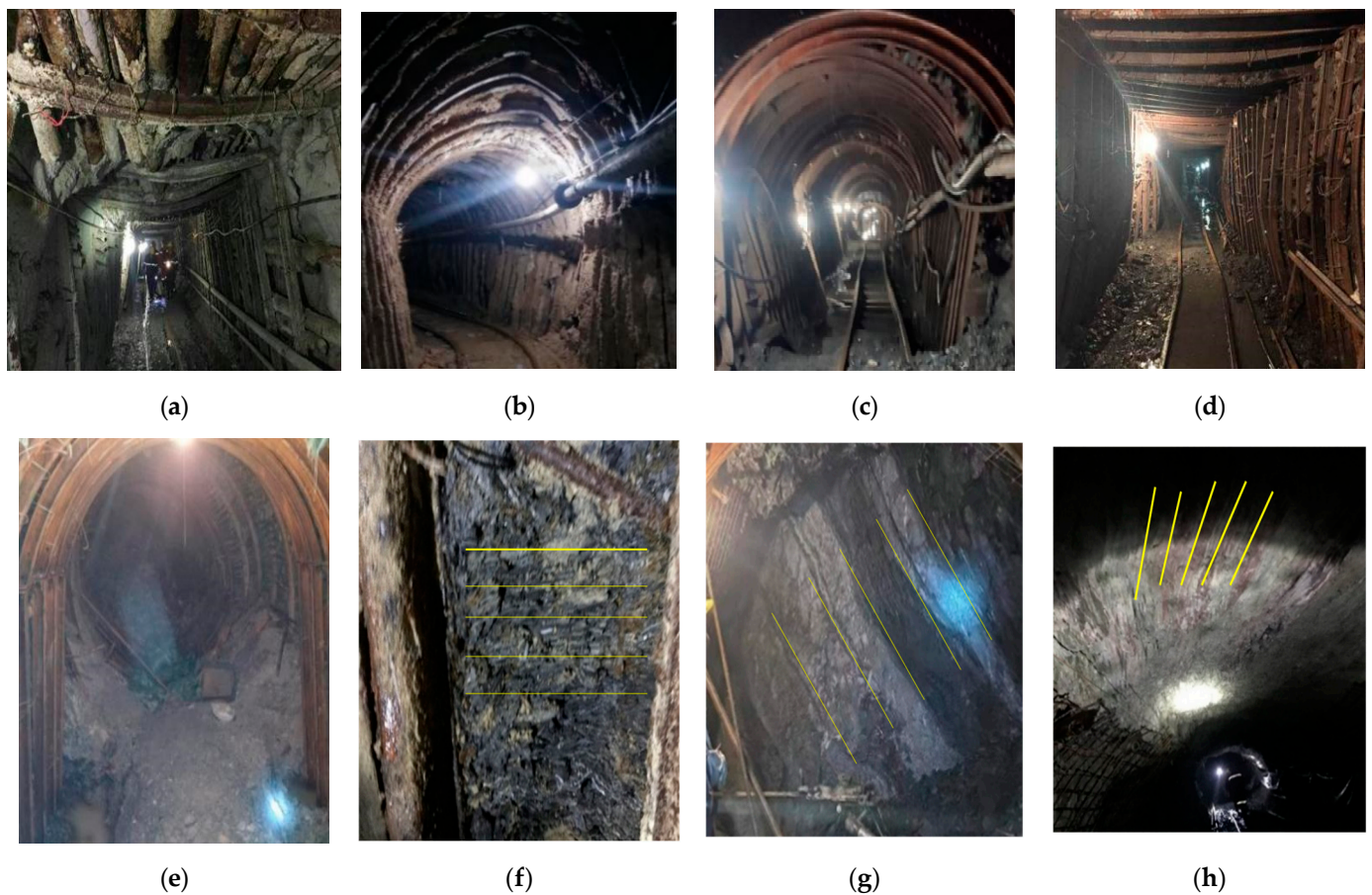
Figure 11. Deformation examples of phyllite roadway support engineering: (**a**) roof settlement, (**b**) roof steel frame bending diagram, (**c**) the feet deformation of a steel frame, (**d**) deformation of a side steel frame, (**e**) large deformation of the floor, (**f**) β = 0°, (**g**) β = 45° and (**h**) β = 90°.

(3) Serious floor heave in the deep roadway.

In the shallow roadway, there were basically no support measures for the floor and the floor heave was not obvious. However, in the deep roadway, if the floor support was not added with a floor beam, the floor deformed before the side and roof, which had a serious impact on ventilation and transportation, and the workload of the floor heave repair was large. The Mengnuo lead–zinc mining area adopts rail transportation, and there are no support measures for the roadway floor above the 450 m middle section, and its floor heave damage is shown in Figure 11e. In the 450 m middle section and below, the roadway floor heave deformation was obvious, which seriously affected transportation and increased the difficulty of roadway maintenance. When the roadway was repaired, the floor heave still had a secondary floor heave after being cut out and reinforced.

(4) The deformation of different bedding dip angles of roadway surrounding rocks varied greatly.

In the lead–zinc mining area, rail transportation was adopted and the roadway was arranged in the footwall of the ore body along the strike of the ore body. Therefore, in a large number of phyllite roadways, the roadway-surrounding rock had different bedding dip angles along the strike of the ore body and the roadway support deformation of different bedding dip angles varied greatly, as shown in Figure 11f–h, which were the bedding dip angles of the roadway-surrounding rock of 0°, 45° and 90°. Among them, deformation occurred after the support of the 0°-bedding surrounding rock. The shotcrete layer fell and weathering occurred. The roadway with 45°- and 90°-bedding surrounding rock was just tunneling for support. Through a large number of field investigations, it was

found that when the roadway surrounding rock was relatively dry and the bedding was at 90°, the roadway could be used after shotcrete and supported by a steel frame, and its deformation is relatively small. When the roadway surrounding rock was at 45°, the roadway deformation was the largest and the deformation speed was the fastest. Therefore, the support must be quickly followed up during roadway excavation. Especially in the case of the fault area and water in the roadway, advanced bolt support was required to ensure the safety of the tunneling construction. From the engineering deformation characteristics of the phyllite roadway surrounding rock with different bedding dip angles, it was difficult to support when the bedding dip angle was 30~60°, which was mainly reflected in the fact that the surrounding rock was easily damaged and deformed by the stress environment itself, and the creep deformation cycle was long. A large number of on-site investigation conclusions were basically consistent with the indoor test conclusions.

Through the above tests and engineering examples, it was fully confirmed that the deformation and damage of different bedding angles of water-saturated phyllite were different. In the actual support process of the water-saturated phyllite roadway, the engineering layout should try to make the included angle between the maximum principal stress and bedding form a 0° or 90° angle in the design stage. During construction, drainage should be carried out first, and then shotcrete should be sprayed to prevent weathering. For the unavoidable bedding of 30~60°, a vertical bedding bolt should be used for reinforcement and support to prevent large deformations caused by dislocation and sliding along the bedding. Long-term creep deformation must be considered. When the bedding dip angle and the maximum principal stress were between 0° and 60°, large deformations could occur under the lower stress disturbance. Moreover, the deformation increased with the stress loading time, and the creep effect was obvious, which was unfavorable to the single rigid support. Therefore, support measures should involve flexible and rigid combination support as much as possible.

5. Conclusions

In this study, the long-term mechanical behavior of phyllite under the coupling effect of a bedding dip, water-saturation condition and stress environment was investigated through a creep test of water-saturated phyllite with different bedding dip angles. The preliminary understanding and conclusions were as follows:

(1) When the bedding dip angle was 30~60°, under the control of the bedding, the phenomenon of sliding along the bedding appeared under the condition of a low-stress constant load, and the slip instantaneous creep deformation suddenly increased, but the sample did not have structural damage and could continuously bear multi-level stress and produce creep deformation. The sudden increase in instantaneous creep deformation had a large destructive effect on the rigid support of the roadway. At this time, it was more suitable to provide a rigid–flexible combination support method.

(2) In the multi-level stress loading process of the creep test, the initial instantaneous stress variable was directly proportional to the size of the loading stress. When the stress was loaded to 50% of the failure strength, the instantaneous stress variable tended to be stable and maintained a linear, slightly increasing relationship with the stress level. When the bedding dip angle was 30~60°, the creep deformation accounted for more than 50% of the total deformation, while the bedding dip angles of 0° and 90° were dominated by the instantaneous strain in the stress loading process. The experimental results clearly showed that the main cause of deep large deformation was the stress environment, and the long-term creep deformation of the roadway was greater when the maximum principal stress and the dip angle of the rock bedding were at 30~60°.

(3) The confining pressure had an obvious influence on the creep failure mode. The uniaxial creep specimens mainly displayed compression shear tensile failure, with a small number of parallel cracks along the main fracture surface. The mode of triaxial creep rupture changed the failure mode to single shear failure. The confining pressure

had a greater inhibitory effect on the creep of samples with bedding dips of 0° and 90°. The creep deformation and failure of samples with bedding dips of 30~60° were mainly controlled by the bedding. Therefore, the main method of phyllite roadway reinforcement is to control the slip of the bedding.

Author Contributions: Y.W. and J.H. wrote the main text of the manuscript. G.W. gathered some of the experimental data. All authors read and agreed to the published version of the manuscript.

Institutional Review Board Statement: Not applicable.

Informed Consent Statement: Not applicable.

Data Availability Statement: The study did not report any data.

Conflicts of Interest: The authors declare no conflict of interest.

References

1. Xie, C.; Nguyen, H.; Bui, X.-N.; Nguyen, V.-T.; Zhou, J. Predicting roof displacement of roadways in underground coal mines using adaptive neuro-fuzzy inference system optimized by various physics-based optimization algorithms. *J. Rock Mech. Geotech. Eng.* **2021**, *13*, 1452–1465. [CrossRef]
2. Xie, C.; Nguyen, H.; Choi, Y.; Armaghani, D.J. Optimized functional linked neural network for predicting diaphragm wall deflection induced by braced excavations in clays. *Geosci. Front.* **2021**, *13*, 101313. [CrossRef]
3. Zhang, X.; Zou, J. Research on collaborative control technology of coal spontaneous combustion and gas coupling disaster in goaf based on dynamic isolation. *Fuel* **2022**, *321*, 124123. [CrossRef]
4. Cao, J.; Xie, C.; Hou, Z. Ecological evaluation of heavy metal pollution in the soil of Pb-Zn mines. *Ecotoxicology* **2022**, *31*, 259–270. [CrossRef]
5. Ramamurthy, T. Engineering performance of phyllite foreign. *Sci. Technol.* **1994**, *25*, 48–52.
6. Chen, Z.; He, C.; Xu, G.; Ma, G.; Wu, D. A Case Study on the Asymmetric Deformation Characteristics and Mechanical Behavior of Deep-Buried Tunnel in Phyllite. *Rock Mech. Rock Eng.* **2019**, *52*, 4527–4545. [CrossRef]
7. Si, X.-F.; Huang, L.-Q.; Li, X.-B.; Gong, F.-Q.; Liu, X.-L. Mechanical properties and rockburst proneness of phyllite under uniaxial compression. *Trans. Nonferrous Met. Soc. China* **2021**, *31*, 3862–3878. [CrossRef]
8. Zhao, J.; Jie, M.; Li, T. Softening effect of phyllite with water saturation. *J. Eng. Geol.* **2017**, *25*, 1449–1454. [CrossRef]
9. Chang, X.; Zhang, X.; Qian, L.; Chen, S.; Yu, J. Influence of bedding anisotropy on the dynamic fracture behavior of layered phyllite. *Eng. Fract. Mech.* **2021**, *260*, 108183. [CrossRef]
10. Xu, G.; Gutierrez, M. Study on the damage evolution in secondary tunnel lining under the combined actions of corrosion degradation of preliminary support and creep deformation of surrounding rock. *Transp. Geotech.* **2020**, *27*, 100501. [CrossRef]
11. Lyu, C.; Liu, J.; Ren, Y.; Liang, C.; Liao, Y. Study on very long-term creep tests and nonlinear creep-damage constitutive model of salt rock. *Int. J. Rock Mech. Min. Sci.* **2021**, *146*, 104873. [CrossRef]
12. Discenza, M.E.; Martino, S.; Bretschneider, A.; Mugnozza, G.S. Influence of joints on creep processes involving rock masses: Results from physical-analogue laboratory tests. *Int. J. Rock Mech. Min. Sci.* **2020**, *128*, 104261. [CrossRef]
13. Ma, L.; Wang, Y.; Wang, M.; Xue, B.; Duan, L. Mechanical properties of rock salt under combined creep and fatigue. *Int. J. Rock Mech. Min. Sci.* **2021**, *141*, 104654. [CrossRef]
14. Xu, G.; He, C.; Chen, Z.; Yang, Q. Transversely isotropic creep behavior of phyllite and its influence on the long-term safety of the secondary lining of tunnels. *Eng. Geol.* **2020**, *278*, 105834. [CrossRef]
15. Tang, H.; Wang, D.; Huang, R.; Pei, X.; Chen, W. A new rock creep model based on variable-order fractional derivatives and continuum damage mechanics. *Bull. Eng. Geol. Environ.* **2017**, *77*, 375–383. [CrossRef]
16. Tang, S.B.; Yu, C.Y.; Heap, M.J. The Influence of Water Saturation on the Short-and Long-Term Mechanical Behavior of Red Sandstone. *Rock Mech. Rock Eng.* **2018**, *51*, 2669–2687. [CrossRef]
17. Yu, C.; Tang, S.; Duan, D.; Zhang, Y.; Liang, Z.; Ma, K.; Ma, T. The effect of water on the creep behavior of red sandstone. *Eng. Geol.* **2019**, *253*, 64–74. [CrossRef]
18. Yi, H.; Zhou, H.; Wang, R.; Liu, D.; Ding, J. On the Relationship between Creep Strain and Permeability of Granite: Experiment and Model Investigation. *Energies* **2018**, *11*, 2859. [CrossRef]
19. Wang, Q.; Hu, X.; Xu, C. Time-dependent behavior of saturated silty mudstone under different confining pressures. *Bull. Eng. Geol. Environ.* **2020**, *79*, 2621–2634. [CrossRef]
20. Bérest, P.; Gharbi, H.; Brouard, B.; Brückner, D.; DeVries, K.; Hévin, G.; Hofer, G.; Spiers, C.; Urai, J. Very Slow Creep Tests on Salt Samples. *Rock Mech. Rock Eng.* **2019**, *52*, 2917–2934. [CrossRef]
21. Yang, S.; Hu, B. Creep and Long-Term Permeability of a Red Sandstone Subjected to Cyclic Loading after Thermal Treatments. *Rock Mech. Rock Eng.* **2018**, *51*, 2981–3004. [CrossRef]

22. Huang, Y.; Li, J.; Ma, D.; Gao, H.; Guo, Y.; Ouyang, S. Triaxial compression behaviour of gangue solid wastes under effects of particle size and confining pressure. *Sci. Total Environ.* **2019**, *693*, 133607. [CrossRef] [PubMed]

23. Yuan, Z.; Zhao, J.; Li, S.; Jiang, Z.; Huang, F. A Unified Solution for Surrounding Rock of Roadway Considering Seepage, Dilatancy, Strain-Softening and Intermediate Principal Stress. *Sustainability* **2022**, *14*, 8099. [CrossRef]

24. Zhan, X.; Zhang, P.; Wen, Z.; Ma, Z.; Kong, D.; Kang, X.; Han, S. Study on the Dip Angle Effect of Asymmetric Deformation and Failure of the Gob-Side Coal–Rock Roadway in Gently Inclined Coal Seam. *Sustainability* **2022**, *14*, 7299. [CrossRef]

25. Wang, Z.; Zhang, J.; Li, J.; Wang, P.; Wu, C.; Shi, L. Research of Surrounding Rock Control of Gob-Side Entry Retaining Based on Deviatoric Stress Distribution Characteristics. *Sustainability* **2022**, *14*, 5660. [CrossRef]

26. Wu, H.; Jia, Q.; Wang, W.; Zhang, N.; Zhao, Y. Experimental Test on Nonuniform Deformation in the Tilted Strata of a Deep Coal Mine. *Sustainability* **2021**, *13*, 13280. [CrossRef]